How to cite: *Angew. Chem. Int. Ed.* **2023,** *62,* e202217808
doi.org/10.1002/anie.202217808

Porous Carbon | Hot Paper

When High-Temperature Cesium Chemistry Meets Self-Templating: Metal Acetates as Building Blocks of Unusual Highly Porous Carbons

Jiaxin Li, Janina Kossmann, Ke Zeng, Kun Zhang, Bingjie Wang, Christian Weinberger, Markus Antonietti, Mateusz Odziomek, and Nieves López-Salas**

Abstract: Self-templating is a facile strategy for synthesizing porous carbons by direct pyrolysis of organic metal salts. However, the method typically suffers from low yields (<4%) and limited specific surface areas (SSA < 2000 $m^2 g^{-1}$) originating from low activity of metal cations (e.g., K^+ or Na^+) in promoting construction and activation of carbon frameworks. Here we use cesium acetate as the only precursor of oxo-carbons with large SSA of the order of 3000 $m^2 g^{-1}$, pore volume approaching 2 $cm^3 g^{-1}$, tunable oxygen contents, and yields of up to 15%. We unravel the role of Cs^+ as an efficient promoter of framework formation, templating and etching agent, while acetates act as carbon/oxygen sources of carbonaceous frameworks. The oxo-carbons show record-high CO_2 uptake of 8.71 mmol g^{-1} and an ultimate specific capacitance of 313 F g^{-1} in the supercapacitor. This study helps to understand and rationally tailor the materials design by a still rare organic solid-state chemistry.

[*] J. Li, Dr. J. Kossmann, Prof. K. Zeng, Prof. M. Antonietti, Dr. M. Odziomek, Dr. N. López-Salas
Colloid Chemistry Department,
Max Planck Institute of Colloids and Interfaces
Am Mühlenberg 1, 14476 Potsdam (Germany)
E-mail: mateusz.odziomek@mpikg.mpg.de
nieves.lopezsalas@mpikg.mpg.de

Prof. K. Zeng
State Key Laboratory of Polymer Materials Engineering, College of Polymer Science and Engineering, Sichuan University
Chengdu 610065 (P. R. China)

K. Zhang, Prof. B. Wang
Laboratory of Advanced Materials, State Key Laboratory of Molecular Engineering of Polymers, and Department of Macromolecular Science, Fudan University
Shanghai 200438 (P. R. China)

Dr. C. Weinberger
Department of Chemistry, Paderborn University
Warburger Str. 100, 33098 Paderborn (Germany)

Introduction

Porous carbons are essential for many fields, including energy storage/conversion, catalysis, and adsorption/separation, owing to their tunable textural properties, rich surface functionalities, and superior stability.[1] The rational design of porous carbons (e.g., porosity and surface chemistry) is vital for advancing their performances toward different applications. For example, microporous carbons with high specific surface areas (SSA > 2000 $m^2 g^{-1}$) and moderate nitrogen/oxygen functionalization are well-suited for adsorption and electrocatalytic reactions of small molecules.[1] The meso-/macro-pores can facilitate mass transfer, making the active surfaces more accessible and being favorable for supercapacitors, batteries, and (electro)catalysts.[2]

Producing highly porous carbons simply and efficiently is desirable for their large-scale applicability. Currently, they are mainly synthesized either by activation or templating strategies.[1b,3] Traditional activation strategy is rather complex and time-consuming, which requires etching of carbon materials with abundant corrosive agents (e.g., potassium (K) and sodium (Na) hydroxides) or high-temperature media (e.g., CO_2, O_2, and H_2O), typically obtaining microporous carbons.[3] In contrast, mesostructured carbons are mainly obtained by soft or hard templating methods.[4] However, they come with drawbacks like a complex template synthesis (e.g., SBA-15) or template removal with harsh chemicals (e.g., hydrofluoric acid). Self-template represents a promising approach towards the facile synthesis of porous carbons by direct calcination of single commercial precursors (e.g., metal citrate and carboxyl salts).[5] However, the reported K or Na-based precursors suffer from low carbon yields (<4%) and limited SSAs (< 2000 $m^2 g^{-1}$). This is mainly because K and Na salts exploited in these cases have a minor impact on the formation and activation of carbon networks.[6]

In contrast to that, cesium (Cs) salts can effectively facilitate the formation of carbon networks and, at the same time, exhibit superior activation properties compared with K and Na.[7] The "cesium effect" is a term well-known in organic chemistry describing milder reaction conditions and higher yields in the presence of Cs^+ ions.[8] The effect is rather empirical and not well understood. Most of the explanations relate the performance to the larger ionic radius of Cs^+, thus to its larger polarizability and being less prone to ion-pairing in solution. This makes Cs^+ a more

efficient catalyst of nucleophilic substitutions in comparison with K^+ or Na^+. Moreover, cesium salts, such as cesium carbonate (Cs_2CO_3), are crucial for C–H activation and C–H/C–O biaryl coupling, increasing the yield three times compared with K_2CO_3 as a catalyst.[8f] Therefore, the effect is not solely related to the increased basicity of Cs species compared with K or Na, as one might think. All of that make Cs organic compounds particularly interesting as the precursors of carbonaceous materials. Changing K or Na organic salts toward Cs are promising to greatly enhance the carbon yields and SSAs simultaneously.

As a matter of fact, cesium acetate (CsAc) has already been used in synthesizing carbon materials, but only as a porogen.[9] The authors described the formation of highly porous carbons, not taking into account the possibility that CsAc itself is a donor of carbon atoms into the carbon lattice. Inspired by the above facts, we assumed that the "cesium ion effect" could be exploited for the construction of covalent networks and explored it during condensation of the simplest organic cesium salt, CsAc.

Here we discover that CsAc can act as a single precursor for highly porous carbons with adjustable SSAs (1000–3000 $m^2 g^{-1}$), multiple scale pore structures, and tunable level of oxygen atoms (7–12 wt %) in the absence of any other additives. Our results challenge the conventional understanding of the role of metal acetates in the synthesis of porous carbons.[10] Mechanistic studies show that during thermal pyrolysis, Cs activates the acetate anions, most likely by forming highly reactive ketene moieties which condense, forming the carbonaceous frameworks around in situ generated Cs species (e.g., Cs_2CO_3, Cs oxides, and Cs), thus acting as built-in templates of meso- and macro-pores. Cs species later also act as powerful chemical activating agents to generate a large volume of micro- and meso-pores. Remarkably, despite the absence of N species, the final carbons are very effective in CO_2 sorption (8.71 mmol g^{-1}, up to 38 wt % of adsorbent itself) and energy storage (313 F g^{-1}) in supercapacitors. This work offers a fundamental understanding of the formation of highly porous carbons from alkali metal acetate salts. The unique role of Cs in a whole process is confirmed by carbonizing potassium, sodium, and zinc acetates. The former produced carbons with SSA of 2000 $m^2 g^{-1}$ but in low yield (<4%), while sodium and zinc acetates did not generate any carbon residue.

Results and Discussion

Pyrolysis behavior of CsAc

Typically, porous oxo-carbons are obtained by heating CsAc to 450–800 °C in a nitrogen atmosphere and subsequent acid washings (Figure 1a). To understand the formation mechanism of porous carbons, we first investigated the decomposition profile of CsAc by thermogravimetric analysis (TGA) and the evolved volatile species by the coupled mass spectrometer (MS) (Figure 1b). CsAc keeps thermally stable until 390 °C, after which it experiences the first steep mass loss of ≈31 % accompanied by the release of a large amount of hydrogen (H_2, $m/z=2$) and concomitant water (H_2O, $m/z=18$). This indicates the rapid condensation of organic species (crosslinking and cyclization of polyketones) and the formation of carbonaceous matter (dehydrogenation and aromatization), which was also observed during the condensation of biomass.[11] We will show later that the

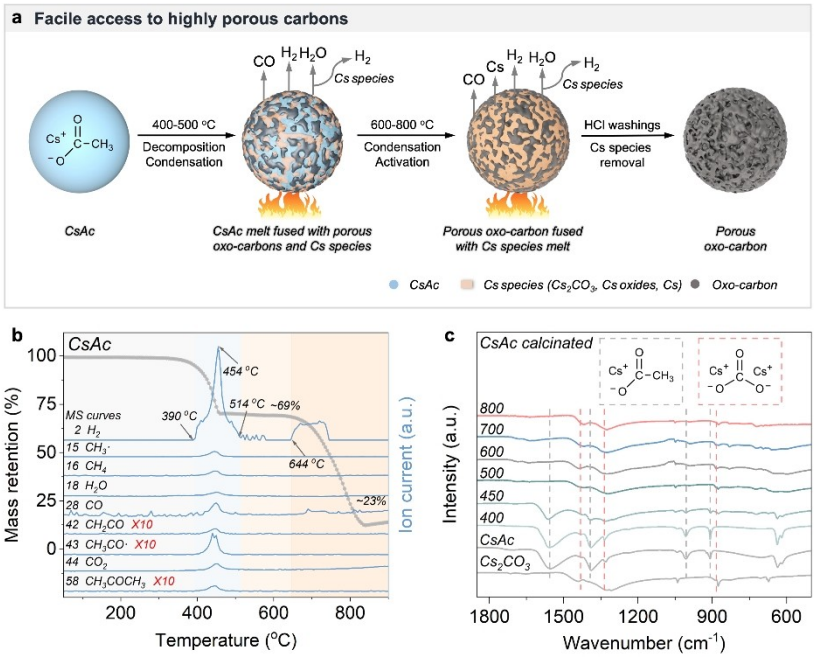

Figure 1. Mechanism of porous carbon formation during pyrolysis of CsAc. a) Scheme of the process with depicted conditions of thermal treatment. b) TGA-MS curves of CsAc under helium. c) Fourier transform-infrared spectra recorded ex situ at different temperatures.

formation of H_2 is also likely favored by eliminated water with metallic Cs. Acetates have been reported to decompose to acetone and further to ketene and to methane at high temperatures.[12] Therefore, the ionic currents at $m/z = 58$, 43, 42, 16, and 15 are assigned to acetone (CH_3COCH_3), the acetate fragment ($CH_3CO^{\bullet}$), ketene (CH_2CO), methane (CH_4), and the methyl fragment ($CH_3^{\bullet}$), respectively. Ketenes are highly reactive and rapidly polymerize, forming polyketone chains that further cross-link towards carbonaceous frameworks.[13] The cross-linking process generates the abovementioned water molecules. The acetone condensation is an alternative pathway contributing to carbon frameworks (Figure S1). Particularly, all these processes are accelerated by Cs^+ ions ("cesium ion effect"), encouraging the formation of carbonaceous networks instead of releasing the gaseous products out of the reaction medium. Cs^+ ions can also stabilize the polyketone moieties by favoring their enolate form and catalyzing intra- and inter-molecular crosslinking and aromatization reactions (Figure 2). This is particularly facilitated by the larger atom radius of Cs than K, Na, and Li.

The solid pyrolysis products obtained at several temperatures (400–800 °C) without washings are carefully analyzed. This is to be separated from the later part focusing on analysing the collected carbons after washing. The transformation of CsAc into Cs_2CO_3 is confirmed by ex situ Fourier transform infrared spectroscopy and X-ray diffraction (Figures 1c and S2). The infrared spectrum of pyrolysis products at 400 °C corresponds well to that of pristine CsAc, while it matches that of Cs_2CO_3 at 500 °C; the mixture of the two is observed at 450 °C. X-ray diffraction spectra perfectly agree with the above results, showing the complete disappearance of characteristic peaks of CsAc and the appearance of the carbonate phase at 500 °C. It is worth mentioning that the whole process of carbon network construction and Cs_2CO_3 formation takes place in homogeneous molten salt because CsAc melts already below 200 °C. This is favorable for the homogeneity of the final products. The alkali metals like K and Na have already been observed during the activation process of carbonaceous matter, however, at higher temperatures (K at 500 °C, and Na at 730 °C).[14] Calculations of Gibbs free energy of theoretical reactions between Cs species with simple aliphatic moieties rationalize the assumption of hydrocarbon thermal reduction of metallic Cs (Table S1). Therefore, we expect that metallic species might emerge at even lower temperatures. The abrupt release of H_2 between 400 and 500 °C is thus connected to the fast condensation of organic species and supposed reaction between metallic Cs with water, while the activation of carbonaceous matter may also contribute to the generation of H_2.

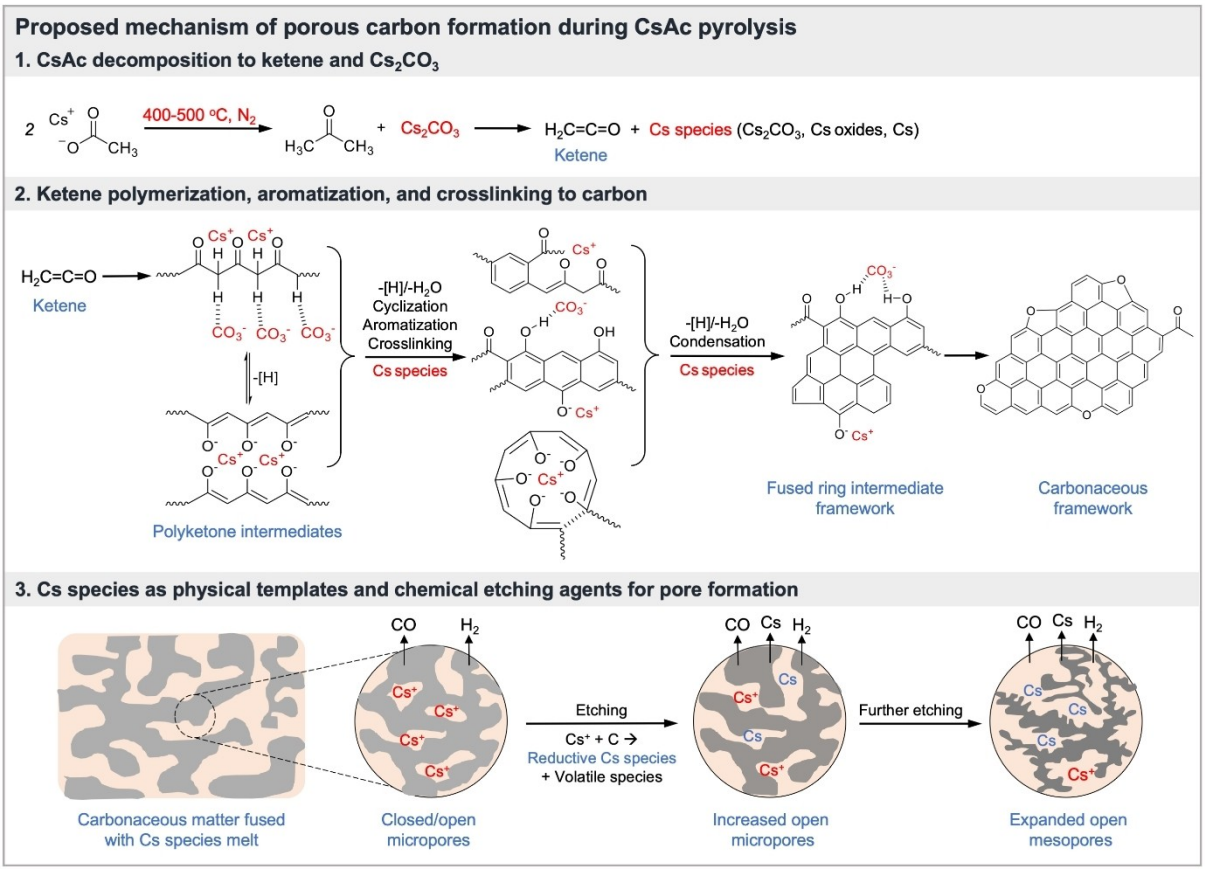

Figure 2. Proposed mechanism of porous carbon formation during CsAc pyrolysis.

No obvious mass loss and gas formation are observed between 520 and 640 °C, pointing at minor chemical evolution of carbon networks in this temperature range. The second sharp mass loss takes place from 650 to 810 °C with H_2 and CO evolution, indicating an intensive activation process by Cs species (e.g., Cs_2CO_3, Cs oxides, or metal). As a supplement, TGA-MS curves indicate that a pure Cs_2CO_3 decomposes from 600 °C on (melting point: 610 °C) with a strong mass loss and increasing CO_2 evolution from 700 °C (Figure S3). This points to the in situ generation of Cs_2O which however is not stable at this temperature and is reported to convert metallic Cs and other oxides further acting as etching agents.[15] The released CO_2 also works as an etching medium at such temperatures (Table S1). The sharp mass drop below 25 % of the initial mass both in the case of CsAc and Cs_2CO_3 is associated with the evaporation of volatile Cs species (boiling point of metallic Cs: 671 °C). Note the in situ generated Cs oxides are extremely unstable, air-sensitive, and hygroscopic, which rapidly convert to Cs_2CO_3 when exposed to the air. The reactive metallic Cs also instantly transform into Cs oxides in the air and then Cs_2CO_3 when reacting with CO_2 or carbon networks. Therefore, we have not been able to detect them in the ex situ structural analysis of solid pyrolysis products. The emerged D and G bands in Raman spectra of unwashed products evidence the formation of carbon frameworks starting from 450 °C (Figure S4). Scanning electronic microscopic image of unwashed CsAc450 show that some colloid particles are encapsulated in a continuous phase (Figure S5), confirming the homogeneous nucleation of carbon frameworks from the salt melt. The calcination products are rather homogeneous at higher temperatures, implying that Cs species are fully fused with carbonaceous scaffolds.

Characterizations of porous oxo-carbons

The structural and chemical transformations of porous carbons were further examined. For that, the materials were first thoroughly washed with an acidic solution to remove the remaining Cs species. The yields of obtained carbonaceous materials were 15–10 % at 500–800 °C, which are higher than the other reported organic metal precursors.[5] Scanning electron microscopic images (Figures 3a–c and S6) show that the frameworks are made up of primary colloidal particles (100–200 nm) that fuse or tightly stack together into grape-like aggregates forming three-dimensional networks including colloidal interconnected voids (0.5–2.0 μm). This morphology is often but not always observed in salt melt synthesis of porous carbons when precursors can dissolve in the ionic melt before condensation occurs and then experience homogeneous nucleation to form carbona-

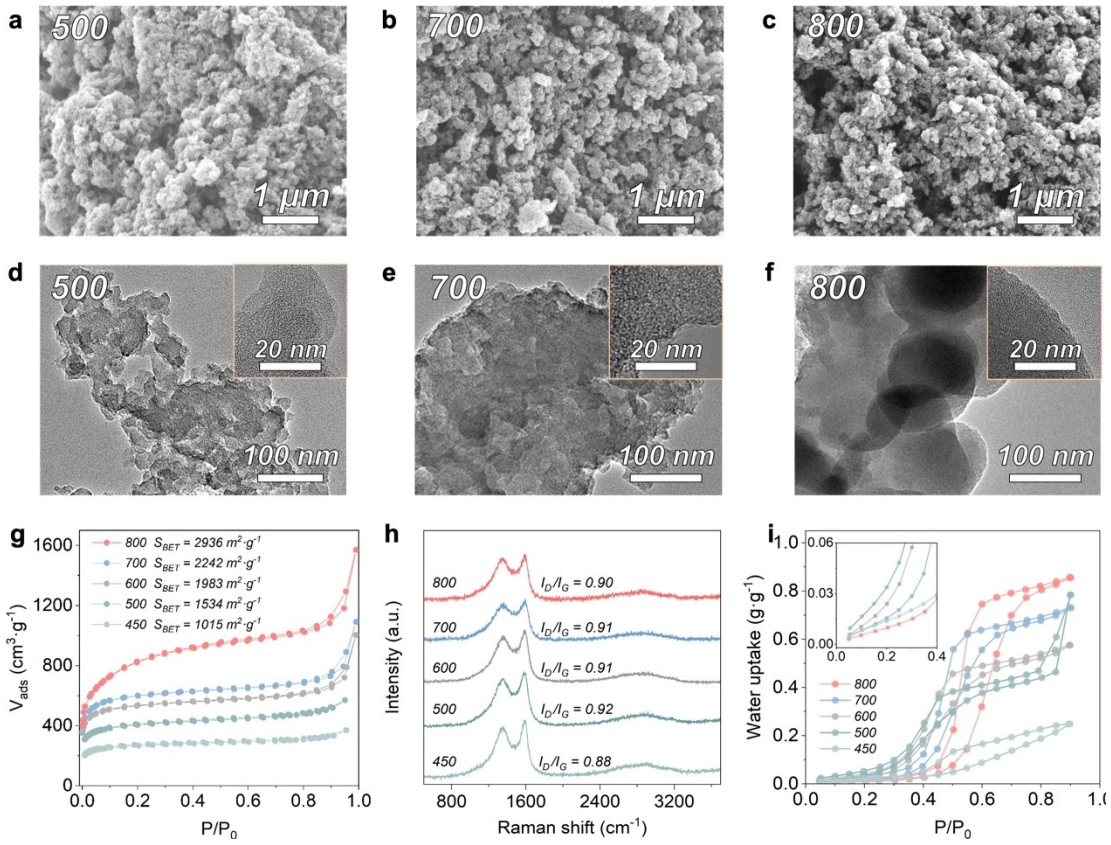

Figure 3. Structural characterizations of porous oxo-carbons at different temperatures. a)–c) Scanning electron microscopic and d)–f) transmission electron microscopic images of samples obtained at a), d) 500, b), e) 700, and c), f) 800 °C. g) N_2 adsorption/desorption isotherms at 77 K, h) Raman spectra and i) water adsorption/desorption isotherms at 298 K (inset, the water uptake at low relative pressure).

ceous materials from the salt melt.[1d,2d–e] In our method, we do not need to dissolve anything because CsAc acts as precursor and salt melt at the same time. Transmission electron micrographs of the products obtained between 500 and 700 °C (Figure 3d–f and S7) show the interconnected colloidal particles, while CsAc800 has smooth surfaces probably because the molten Cs species preferentially etch away irregularities outside the colloidal particles.

The pore structure of the carbons was further evaluated by N_2 sorption measurements at 77 K (Figure 3g). All the sorption isotherms feature a rapid N_2 uptake at low relative pressures ($P/P_0 < 0.01$), indicating the existence of large volumes of micropores. At higher relative pressures, the isotherms of products calcined between 600 and 800 °C show the features of the model Type II isotherm with a gradual increase of N_2 adsorption without reaching a clear plateau near P/P_0 of 0.9. Type II isotherm is characteristic of large mesopores and/or macropores. In addition, CsAc800 shows a steeper uptake in the relative pressure range from 0.3 to 0.6, suggesting the formation of small mesopores. As listed in Table 1, the samples present gradually increasing Brunauer–Emmett–Teller (BET) SSAs of 1015, 1534, 1983, and 2242 $m^2 g^{-1}$ at 450, 500, 600, and 700 °C, reaching up to 2936 $m^2 g^{-1}$ at 800 °C. The pore size distributions calculated from quenched solid density functional theory (QSDFT) adsorption equilibrium kernels are depicted in Figure S8. All the samples show hierarchical porous structures comprising large micropores (1–2 nm), small mesopores (2–4 nm), and large mesopores (20–40 nm). CsAc450 owns a pore volume of 0.53 $cm^3 g^{-1}$, indicating effective construction and activation of carbon frameworks at a mild temperature. The pore volume increases to 0.90, 1.13, 1.29, and 1.89 $cm^3 g^{-1}$ at 500, 600, 700, and 800 °C, respectively. The obtained carbons are micropore-dominated below 800 °C, while CsAc800 owns comparable micropore and mesopore volumes (0.99 and 0.90 $cm^3 g^{-1}$).

The chemical structures of obtained carbons were also carefully studied. X-ray diffraction pattern of CsAc450 shows one broad and low-intensity diffraction peak centered at 24° approximately characteristic of stacking (Figure S9); no visible peaks are observed for samples obtained at higher temperatures, indicating their amorphous porous structures. Raman spectra show typical D (≈1350 cm^{-1}) and G (≈1580 cm^{-1}) bands (Figure 3h), usually corresponding to the disordered and ideal graphitic vibrations of the carbons. The high I_D/I_G values are typical for poorly ordered carbon structures, as they often exist in highly porous, bent carbons with asymmetric heteroatom substitution. This is consistent with X-ray diffraction results. Elemental combustion analyses show that the samples have tunable oxygen contents (6.8–12.5 wt %) (Table 1), indicating the role of acetates as carbon and oxygen sources. The content of oxygen remains stable between 450 and 600 °C, in accordance with TGA-MS analyses (Figure 1b) in which no mass loss was observed. As expected, the oxygen content decreases at higher temperatures due to the elimination of C=O by cesium-etching.

The infrared spectra further probe the surface chemical functionalities of the obtained carbons (Figure S10). CsAc450 shows a broad peak at ≈1700 cm^{-1} attributed to the vibrations of C=O groups in polyketone-derived intermediates, a broad peak at ≈1600 cm^{-1} related to the conjugated carbon networks, a broad peak between 1400 and 950 cm^{-1} related to the stretching vibrations of C–O and bending vibration of C–H bonds. With increasing temperature, the signals of C=O, C–O, and C–H regions gradually weaken and vanish at 800 °C, indicating the formation of an extended conjugated structure of carbon frameworks. Water sorption at 298 K of all the samples present a Type V isotherm with limited uptake below $P/P_0 = 0.3$ (Figure 3i), indicating weak interaction between carbon pore walls with water molecules; a large hysteresis loop are related to mesopores. CsAc800 shows the lowest water uptake at low pressures owing to fewer hydrophilic groups (e.g., carboxyl groups) on the surface, and a maximum water uptake of 0.86 $g_{H_2O} g^{-1}$ is in agreement with its high mesopore volume.

^{13}C solid-state nuclear magnetic resonance spectrum of CsAc450 further confirms the presence of sp^3 hybrid aliphatic and sp^2 aromatic carbon (Figure S11), in good agreement with the polyketone and the acetone-aldol condensation mechanism. X-ray photoelectron survey spectra (Figure S12) show that the carbons have two significant O 1s and C 1s peaks, consistent with the elemental chemical analysis results. Further deconvolution of high-resolution C 1s spectra (Figure S13) indicates that the carbons contain C=C (≈284.6 eV), C–O (≈286.4 eV), and C=O (≈288.8 eV) groups. No noticeable intensity changes in the

Table 1: Elemental compositions and textural properties of porous oxo-carbons obtained at different temperatures.

Samples	C[a] [wt %]	H[a] [wt %]	O[a] [wt %]	Cs[b] [wt %]	S_{BET}[c] [$m^2 g^{-1}$]	V_{Micro}[d] [$cm^3 g^{-1}$]	V_{Meso}[d] [$cm^3 g^{-1}$]	V_T[e] [$cm^3 g^{-1}$]	H_2O uptake at $P/P_0 = 0.3$[f] [$g g^{-1}$]	Max H_2O uptake[f] [$g g^{-1}$]	Max CO_2 uptake[g] [mmol g^{-1}]
CsAc450	85.5	2.5	12.3	0.2	1015	0.33	0.17	0.53	0.020	0.25	3.80
CsAc500	86.2	1.4	12.2	0.2	1534	0.53	0.34	0.90	0.072	0.78	5.97
CsAc600	88.0	1.0	11.0	0.2	1983	0.64	0.49	1.13	0.057	0.58	8.71
CsAc700	88.7	0.9	9.2	0.1	2242	0.73	0.56	1.29	0.028	0.73	6.82
CsAc800	91.2	0.5	6.8	0.1	2936	0.99	0.90	1.89	0.015	0.86	7.21

[a] Chemical compositions from elemental combustion analysis (C, H, O). [b] Metal contents from inductively coupled plasma atomic emission spectroscopy. The contents of C/H, O, and Cs were measured by different modes/methods, and the mass ratio sum of the above elements is not always equal to 100%. [c] Specific surface areas obtained via the multipoint BET model applied to N_2 adsorption isotherm at 77 K in the P/P_0 from 0.05 to 0.25. [d] Micropore and mesopore volumes calculated from the N_2 adsorption/desorption isotherms at 77 K using the QSDFT model. [e] Total pore volumes estimated from the volume adsorbed at P/P_0 of ca. 0.90. [f] Water uptake capacity obtained at 298 K. [h] CO_2 uptake capacity obtained at 273 K.

above groups are observed at higher temperatures. O 1s spectra of CsAc450 contain C=O (≈531.8 eV, O doubly bonded to aromatic carbon) and C–O groups (≈533.3 eV, O singly bonded to aromatic carbon), supporting again the ketene and the acetone polymerization path (Figure S14). With increasing temperature, O peaks shift to the higher binding energy, which can be explained by the conversion of C=O to C–O at higher temperatures on the carbon surfaces. This goes extremely well with the reduction of Cs and the liberation of H_2, leaving a more electropositive character to the frameworks, here mostly localized at the oxygen atoms. The shift by about 1 volt on average is massive, that is, the final material is electron poor.

To show the unique Cs effect in the structural evolution of acetates, some common metal acetic salts were chosen and compared. NaAc-derived carbon at 800 °C has a negligible yield of 0.1 % and quite-low SSA of 212 $m^2 g^{-1}$ (Figure S15) and no carbonaceous matter was obtained after pyrolysis of LiAc and $ZnAc_2$, indicating their incomparable properties with CsAc. KAc-derived carbons show lower yield (4 %), SSA (2038 $m^2 g^{-1}$), pore volume (0.96 $cm^3 g^{-1}$), and consequently lower CO_2 uptake (5.85 mmol g^{-1}) than those from CsAc (Figure S16 and Table S2). KAc releases similar volatile species to CsAc (e.g., H_2, CO, and H_2O) and converts to K_2CO_3 at 500 °C, implying a similar decomposition pathway to CsAc. However, Cs-mediated condensation and activation are more efficient than K. As a proof, both the first and second mass loss of CsAc occur at lower temperatures (390 and 640 °C) those of KAc (400 and 700 °C). Finally, the mass retention of CsAc has reached a steady state at 800 °C while KAc cannot reach the final state at 900 °C, indicating faster activation with Cs species (Figures 1b and S17). The above results highlight the important role of Cs^+ ions in promoting the construction of carbonaceous frameworks (crosslinking and aromatization of polyketones) and the development of porosity (Cs^+ ions as powerful templating and activating agents).

Such specific catalytic effect of Cs species (superior to K or Na) is well recognized in organic chemistry and denoted as "cesium effect".[8a–c] The effect is related to the larger ionic radius and higher polarizability of Cs^+ ions than the other homologous ions (Table S3). This makes Cs^+ ions more efficient catalysts for e.g. nucleophilic substitution and C–H activation than K^+ and Na^+ ions.[8f,g] These reactions are also important for the condensation of organic species to form carbonaceous networks. The rigid carbon frameworks further support the formation of nanopores, important for high SSAs. Besides, the low melting points of Cs species (e.g., Cs_2CO_3, Cs oxides) are also associated with "cesium effect", which guarantees full filtration of molten Cs species into porous carbonaceous scaffold for efficient activation, contributing to high SSAs. For instance, the melting point of Cs_2CO_3 is 610 °C while for K_2CO_3 it is 891 °C. In comparison, K^+ and Na^+ ions are less efficient to accelerate the above processes, and the poor contact and sluggish mass transfer between solid K or Na species and carbons also hinder the activation process. Therefore, higher yields and higher SSAs can be achieved in the presence of a Cs-based precursor simultaneously.

Overall, CsAc plays multiple roles in the process of formation of porous carbons (Figure 2): (i) carbon/oxygen source, (ii) condensation catalyst, (iii) in situ physical template, and (iv) activating agent. CsAc decomposes generating ketene, ketonic species, and Cs_2CO_3 in the range of 400–500 °C. Ketenes rapidly polymerize into polyketones,[14] while Cs^+ and CO_3^{2-} ions most likely coordinate with oxygen groups and the acidic alkyl hydrogen atoms of polyketone chains, respectively. This promotes their crosslinking, cyclization, and aromatization forming oxygen-rich carbonaceous networks. Note that the carbonaceous matter and Cs species are always generated simultaneously in intimate contact, and thus the in situ nucleating Cs_2CO_3 indeed act as a hard template and etching agent. Abundant closed and open pores have been formed at this stage. At around 600 °C, Cs_2CO_3 melts and partly decomposes producing Cs oxides and metal, all of which can work as etching agents to increase the number of open micropores. At 800 °C, the increased reactivity and intense volatilization of Cs species further create open micro- and meso-pores. Some possible etching reactions involving Cs species are provided in Table S1 based on standard Gibbs free energy calculations, and the corresponding data of K species are also calculated for comparison.[16] The activation reactions with K species are also thermodynamically feasible like those with Cs species, while the activation reactions of Cs species are more kinetically favorable owing to effective contact and fast mass transfer between molten Cs species and carbons. The Cs^+ ions enable the synergetic and efficient progression of condensation and activation of the carbonaceous frameworks, which is vital for creating highly porous structures.

Compared with previous synthesis strategies of porous carbons (e.g., carbonization-activation, template-assisted carbonization, self-activation, and combined methods) (Table S4), our strategy is highly facile, efficient, and economical to reach decent yields and ultrahigh SSAs and avoids the demands of large amounts of complex reagents, expensive templates, and tedious process. This proposed approach shows high potential for further academic research and practical applications.

CO_2 adsorption

The ultrahigh microporosity and tunable oxygen contents inspired us to investigate CO_2 capture performance of the porous carbons (Figure 4a). CsAc500 shows a CO_2 adsorption capacity of 5.97 mmol g^{-1} at 273 K and 100 kPa; the value increases to 8.71 mmol g^{-1} for CsAc600, 6.82 mmol g^{-1} for CsAc700, and 7.21 mmol g^{-1} for CsAc800. At 298 K, the capacity decreases to 4.14–4.70 mmol g^{-1} owing to the exothermic nature of the adsorption process (Figure S18). Then, the isosteric heats of adsorption (Q_{st}) were calculated between 15.0–30.0 kJ mol^{-1} based on the Clausius-Clapeyron equation (Figure S19), indicating the *van der Waals* interactions between CO_2 and carbons. The samples at 500 and 600 °C present higher Q_{st} values at low uptake amounts than those at 700 and 800 °C, which is related to the differences in

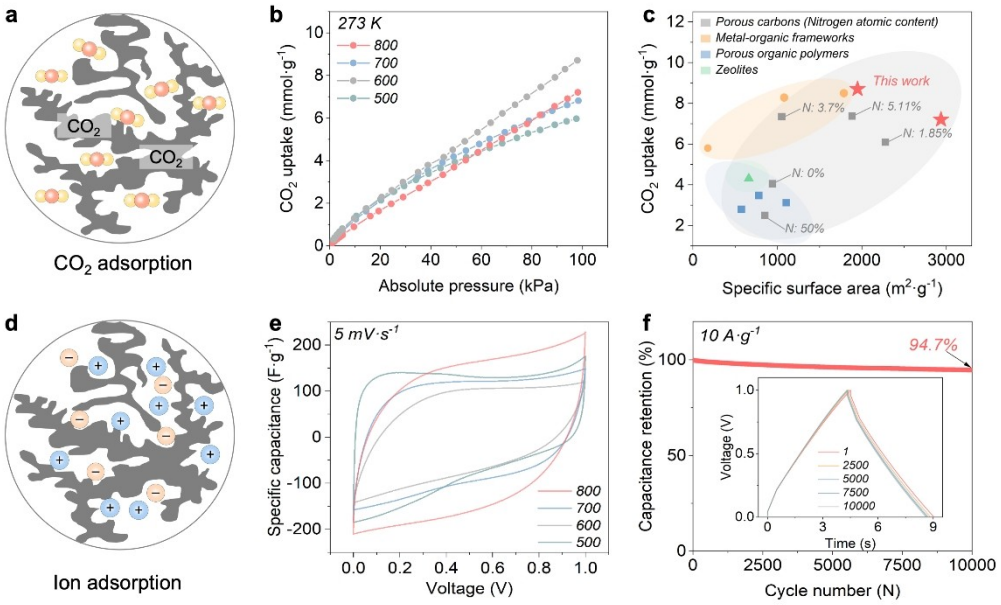

Figure 4. Application demonstrations of porous oxo-carbons obtained from CsAc. a), d) Schemes of porous carbons as CO_2 adsorbent and supercapacitor electrode. b) CO_2 adsorption isotherms at 273 K. c) Specific surface areas and CO_2 uptake comparison with some reported adsorbents (involving Refs. [17–20]). e) Cyclic voltammetry curves of oxo-sxacarbons at 5 mV s^{-1}. f) Capacitance retention over 10000 cycles of CsAc800 at 10 A g^{-1}. Inset image, the selected charge-discharge curves at different cycles.

the content and type of surface oxygen functional groups of the carbons obtained at varied temperatures.

Compared with the reported CO_2 adsorbents (e.g., porous carbons,[17] metal-organic frameworks,[18] zeolites,[19] and porous organic polymers),[20] our materials show remarkable CO_2 sorption capacities (up to 38 wt % of carbon itself under ambient conditions) but avoid the use of complicated precursors and tedious synthesis (Figure 4c and Table S5). Pore size distributions obtained from CO_2 adsorption isotherms at 273 K shows the presence of ultra-narrow micropores (<0.8 nm) (Figure S20), which are known for their affinity towards CO_2 owing to the stronger interaction between the adsorbates and the two adjacent pore walls.[21] The high adsorption capacity is rationally ascribed to the high micropore volumes, and the large amounts of mesopores promote CO_2 diffusion to the inner surfaces of the micropores. Besides textural properties, the oxygen functional groups also provide an increased affinity to CO_2.[22] CsAc600 achieves the highest CO_2 uptake probably for its striking a balance between high micropore volume and still high oxygen content. Further, the adsorption amount remains stable over five adsorption/desorption cycles at 273 K (Figure S21), demonstrating good stability and reusability. High CO_2 uptake is not just favorable for direct CO_2 sorption but also for CO_2 conversion in electrosynthesis or metal-CO_2 batteries.[23]

Supercapacitor

The morphology of colloid particles, high SSAs, and hierarchical pores of oxo-carbons is also favorably instrumentalized for energy storage in supercapacitors based on surface sorption and pseudocapacitive reactions (Figure 4d). The energy-storage behaviors of as-prepared porous carbons were tested in two-electrode symmetric supercapacitors with 1 M H_2SO_4 aqueous electrolyte in Swagelok cells. Cyclic voltammogram curves of the samples show quasi-rectangular shapes (Figures 4e and S22), indicating the electric double-layer capacitances at electrode-electrolyte interfaces and pseudo-capacitances originated from oxygen functionalization, with a clearer contribution of the later at lower temperatures. Galvanostatic charge-discharge tests show that CsAc800 has high specific capacitance and rate performance (313 F g^{-1} at 0.1 A g^{-1}, 90 F g^{-1} at 10 A g^{-1}) (Figures S23, and Table S6). No obvious internal resistance drop is observed in the charge-discharge curves, indicating effective charge transfer. The pore size distributions obtained from isotherm with high resolution at low partial pressures (Figure S24) indicate that CsAc800 has two populations of supramicropores with sizes of 0.9 and 1.4 nm. Interestingly, the samples prepared at lower temperatures show only supramicropores of ca. 0.9 nm. The high specific capacitance of CsAc800 is rationally ascribed to its large SSA, large supramicropes and small mesopores, and oxygen functionalities. The mesopores can host larger volumes of electrolyte and guarantee favorable ion transfer/diffusion to ensure good rate performance, as shown in the water sorption measurement (Figure 3i). Our materials have shown comparable or higher specific capacitances and rate capability than the top-in-class, reported porous carbons obtained via specially-designed precursors and complex synthesis process[24] (Figure S25 and Table S7). CsAc800 shows superior cycling stability at 10 A g^{-1}, with 94.7 %

capacitance retention after 10000 cycles (Figure 4f). The device finally demonstrates a specific energy of 11 $Wh\,kg^{-1}$ at 25 $W\,kg^{-1}$; at a high specific power of 2500 $W\,kg^{-1}$, a specific energy of 5 $Wh\,kg^{-1}$ can still be retained.

Conclusion

In conclusion, a facile and robust approach was presented for synthesizing porous oxo-carbons with ultrahigh SSAs, large pore volumes, hierarchical pore structures, surface oxygen functionalities, and decent carbon yields by direct pyrolysis of CsAc. Importantly, we have revealed that CsAc is a unique all-in-one precursor that decomposes to presumably ketenes and ketones acting as carbon/oxygen sources and Cs species as in situ formed templating and activating agents. The carbonaceous frameworks are rapidly constructed and activated by in situ generated Cs species embedded within the frameworks, leading to ultrahigh-SSAs porous carbons that were demonstrated to have tremendous potential for CO_2 adsorption and energy storage. This method is industrially feasible due to the use of a simple precursor and steps, which makes it easy to extend the synthesis to various highly porous heteroatom-doped carbons by introducing appropriate heteroatom-containing second precursors (e.g., nitrogen, phosphorus, sulfur, and boron). We also believe that Cs species can be easily recovered and transformed into CsAc again, making the process more sustainable and economical. Overall, our results may provide new insights into the convenient synthesis of novel porous carbons via organic, high-temperature bulk synthesis. As the resulting systems are electron-poor, we expect interesting additional applications in cathodic energy storage and oxidative electrochemistry in general.

Acknowledgements

We gratefully appreciate Antje Völkel for measuring TGA-MS and elemental compositions, Pengzhou Li for transmission electron microscopy, Jessica Brandt for inductively coupled plasma spectroscopy, Katharina ten Brummelhuis for water sorption, Yaolin Xu for X-ray diffraction measurements, Zihan Song for electrochemical measurements, and the Max Planck Society for financial support. M. O. acknowledges Alexander Von Humboldt Stiftung for financial support. This research has received funding from the European Research Council (ERC) under the European Union's Horizon 2020 research and innovation programme, MoMa-STOR (Grant agreement no. 951513). Open Access funding enabled and organized by Projekt DEAL.

Conflict of Interest

The authors declare no conflict of interest.

Data Availability Statement

The data that support the findings of this study are available from the corresponding author upon reasonable request.

Keywords: CO_2 Adsorption · Cesium Acetate · Cesium Effect · Porous Carbons · Supercapacitor

[1] a) H. Wang, Y. Shao, S. Mei, Y. Lu, M. Zhang, J. K. Sun, K. Matyjaszewski, M. Antonietti, J. Yuan, *Chem. Rev.* **2020**, *120*, 9363; b) W. Tian, H. Zhang, X. Duan, H. Sun, G. Shao, S. Wang, *Adv. Funct. Mater.* **2020**, *30*, 1909265; c) G. Singh, J. Lee, A. Karakoti, R. Bahadur, J. Yi, D. Zhao, K. Albahily, A. Vinu, *Chem. Soc. Rev.* **2020**, *49*, 4360; d) N. Fechler, T.-P. Fellinger, M. Antonietti, *Adv. Mater.* **2013**, *25*, 75.

[2] a) X. Qiu, N. Wang, Z. Wang, F. Wang, Y. Wang, *Angew. Chem. Int. Ed.* **2021**, *60*, 9610; b) C. Hu, L. Dai, *Adv. Mater.* **2019**, *31*, 1804672; c) G. Lan, J. Yang, R. P. Ye, Y. Boyjoo, J. Liang, X. Liu, Y. Li, J. Liu, K. Qian, *Small Methods* **2021**, *5*, 2001250; d) J. Kossmann, M. L. O. S-Manjavacas, H. Zschiesche, N. V. Tarakina, M. Antonietti, J. Albero, N. López-Salas, *J. Mater. Chem. A* **2022**, *10*, 6107; e) E. Lepre, S. Rat, C. Cavedon, P. H. Seeberger, B. Pieber, M. Antonietti, N. López-Salas, *Angew. Chem. Int. Ed.* **2023**, *62*, e2022116.

[3] a) J. Yin, W. Zhang, N. A. Alhebshi, N. Salah, H. N. Alshareef, *Small Methods* **2020**, *4*, 1900853; b) J. Wang, S. Kaskel, *J. Mater. Chem.* **2012**, *22*, 23710; c) R. M. Navarro, M. A. Peña, J. L. G. Fierro, *Chem. Rev.* **2007**, *107*, 3952; d) D. W. Kim, H. S. Kil, K. Nakabayashi, S. H. Yoon, J. Miyawaki, *Carbon* **2017**, *114*, 98; e) K. Suresh Kumar Reddy, A. Al Shoaibi, C. Srinivasakannan, *New. Carbon. Mater.* **2012**, *27*, 344; f) G. Lin, R. Ma, Y. Zhou, Q. Liu, X. Dong, J. Wang, *Electrochim. Acta* **2018**, *261*, 49; g) K. Zou, Y. Deng, J. Chen, Y. Qian, Y. Yang, Y. Li, G. Chen, *J. Power Sources* **2018**, *378*, 579; h) M. A. Lillo-Ródenas, D. Lozano-Castelló, D. Cazorla-Amorós, A. Linares-Solano, *Carbon* **2001**, *39*, 751.

[4] a) J. Liu, T. Yang, D. W. Wang, G. Q. Lu, D. Zhao, S. Z. Qiao, *Nat. Commun.* **2013**, *4*, 2798; b) U. Jeong, H. Kim, S. Ramesh, N. A. Dogan, S. Wongwilawan, S. Kang, J. Park, E. S. Cho, C. T. Yavuz, *Angew. Chem. Int. Ed.* **2021**, *60*, 22478; c) L. Peng, H. Peng, Y. Liu, X. Wang, C. Te Hung, Z. Zhao, G. Chen, W. Li, L. Mai, D. Zhao, *Sci. Adv.* **2021**, *7*, eabi7403; d) H. W. Liang, W. Wei, Z. S. Wu, X. Feng, K. Müllen, *J. Am. Chem. Soc.* **2013**, *135*, 16002; e) S. Schacht, Q. Huo, I. G. Voigt-Martin, G. D. Stucky, F. Schüth, *Science* **1996**, *273*, 768; f) Y. Fang, Y. Lv, R. Che, H. Wu, X. Zhang, D. Gu, G. Zheng, D. Zhao, *J. Am. Chem. Soc.* **2013**, *135*, 1524; g) F. Zhang, Y. Meng, D. Gu, Y. Yan, Z. Chen, B. Tu, D. Zhao, *Chem. Mater.* **2006**, *18*, 5279; h) J. Tang, J. Liu, C. Li, Y. Li, M. O. Tade, S. Dai, Y. Yamauchi, *Angew. Chem. Int. Ed.* **2015**, *54*, 588.

[5] a) M. Sevilla, N. Díez, A. B. Fuertes, *ChemSusChem* **2021**, *14*, 94; b) B. Yan, H. Huang, X. Qin, S. Xiu, J. Choi, D. Ko, T. Chen, W. Zhang, B. Quan, G. Diao, X. Jin, Y. Piao, *ACS Appl. Energy Mater.* **2021**, *4*, 13735; c) H. Peng, S. Qi, Q. Miao, R. Zhao, Y. Xu, G. Ma, Z. Lei, *J. Power Sources* **2021**, *482*, 228993; d) S. Wang, J. Miao, B. Ren, Y. Xu, Z. Tian, L. Zhang, Z. Liu, *J. Alloys Compd.* **2022**, *920*, 165946; e) H. Ouyang, C. Fang, Z. Xu, L. Li, G. Xiao, *Nanoscale* **2022**, *14*, 11298.

[6] a) M. Sevilla, A. B. Fuertes, *J. Mater. Chem. A* **2013**, *1*, 13738; b) M. Sevilla, A. B. Fuertes, *ACS Nano* **2014**, *8*, 5069; c) S. Yu, N. Sun, L. Hu, L. Wang, Q. Zhu, Y. Guan, B. Xu, *J. Power Sources* **2018**, *405*, 132; d) Y. Zhang, Q. Ma, H. Li, Y. W. Yang, J. Luo, *Small* **2018**, *14*, 1800133; e) M. Sevilla, G. A. Ferrero, N. Diez, A. B. Fuertes, *Carbon* **2018**, *131*, 193.

[7] a) K. Okada, N. Yamamoto, Y. Kameshima, A. Yasumori, *J. Colloid Interface Sci.* **2003**, *262*, 179; b) J. Zhou, Z. Li, W. Xing, H. Shen, X. Bi, T. Zhu, Z. Qiu, S. Zhuo, *Adv. Funct. Mater.* **2016**, *26*, 7955; c) J. Fujiki, K. Yogo, *Chem. Commun.* **2016**, *52*, 186.

[8] a) G. Dijkstra, W. H. Kruizinga, R. M. Kellogg, *J. Org. Chem.* **1987**, *52*, 4230; b) C. Galli, *Org. Prep. Proced. Int.* **1992**, *24*, 285; c) R. Varala, K. S. Rao, *Curr. Org. Chem.* **2015**, *19*, 1242; d) W. Xu, X. An, Q. Zhang, Z. Li, Q. Zhang, Z. Yao, X. Wang, S. Wang, J. Zheng, J. Zhang, W. Wu, M. Wu, *ACS Sustainable Chem. Eng.* **2019**, *7*, 12351; e) S. Xu, Z. Liao, A. Dianat, S. Park, M. A. Addicoat, Y. Fu, D. L. Pastoetter, F. G. Fabozzi, Y. Liu, G. Cuniberti, M. Richter, S. Hecht, X. Feng, *Angew. Chem. Int. Ed.* **2022**, *61*, e202202492; f) H. Xu, K. Muto, J. Yamaguchi, C. Zhao, K. Itami, D. G. Musaev, *J. Am. Chem. Soc.* **2014**, *136*, 14834; g) A. Banerjee, M. W. Kanan, *ACS Cent. Sci.* **2018**, *4*, 606.

[9] a) N. Fechler, G. A. Tiruye, R. Marcilla, M. Antonietti, *RSC Adv.* **2014**, *4*, 26981; b) K. Elumeeva, J. Ren, M. Antonietti, T.-P. Fellinger, *ChemElectroChem* **2015**, *2*, 584; c) S. Jae Yang, R. Rothe, S. Kirchhecker, D. Esposito, M. Antonietti, H. Gojzewski, N. Fechler, *Carbon* **2015**, *94*, 641.

[10] a) J. Zhang, W. Zhang, H. Zhang, J. Pang, G. Cao, M. Han, Y. Yang, *J. Alloys Compd.* **2017**, *712*, 76; b) J. Dai, S. Tian, Y. Jiang, Z. Chang, A. Xie, R. Zhang, Y. Yan, *J. Alloys Compd.* **2018**, *732*, 222; c) G. Singh, I. S. Ismail, C. Bilen, D. Shanbhag, C. I. Sathish, K. Ramadass, A. Vinu, *Appl. Energy* **2019**, *255*, 113831; d) L. Duan, C. Wang, W. Zhang, B. Ma, Y. Deng, W. Li, D. Zhao, *Chem. Rev.* **2021**, *121*, 14349.

[11] B. Babinszki, E. Jakab, V. Terjek, Z. Sebestyen, G. Varhegyi, Z. May, A. Mahakhant, L. Attanatho, A. Suemanotham, Y. Thanmongkhon, Z. Czegeny, *J. Anal. Appl. Pyrolysis* **2021**, *155*, 105069.

[12] a) F. O. Rice, R. E. Vollrath, *Proc. Natl. Acad. Sci. USA* **1929**, *15*, 702; b) C. D. Hurd, W. H. Tallyn, *J. Am. Chem. Soc.* **1925**, *47*, 1427.

[13] a) F. A. Leibfarth, C. J. Hawker, *J. Polym. Sci. Part A* **2013**, *51*, 3769; b) S. M. Mitchell, K. A. Niradha Sachinthani, R. Pulukkody, E. B. Pentzer, *ACS Macro Lett.* **2020**, *9*, 1046; c) S. Rat, A. Chavez-Sanchez, D. Cruz, M. Antonietti, *ACS Appl. Polym. Mater.* **2021**, *3*, 2588.

[14] a) M. ALillo-Ródenas, D. Cazorla-Amorós, A. Linares-Solano, *Carbon* **2003**, *41*, 267; b) C. Lu, S. Xu, C. Liu, *J. Anal. Appl. Pyrolysis* **2010**, *87*, 282; c) W. Chen, M. Gong, K. Li, M. Xia, Z. Chen, H. Xiao, Y. Fang, Y. Chen, H. Yang, H. Chen, *Appl. Energy* **2020**, *278*, 115730.

[15] A. Band, A. Albu-Yaron, T. Livneh, H. Cohen, Y. Feldman, L. Shimon, R. Popovitz-Biro, V. Lyahovitskaya, R. Tenne, *J. Phys. Chem. B* **2004**, *108*, 12360.

[16] D.-I. B. Rumpf, *Thermochemical Data of Pure Substances*, VCH, Weinheim, **1997**.

[17] a) A. C. Dassanayake, M. Jaroniec, *J. Mater. Chem. A* **2017**, *5*, 19456; b) C. Chen, H. Huang, Y. Yu, J. Shi, C. He, R. Albilali, H. Pan, *Chem. Eng. J.* **2018**, *353*, 584; c) G. Singh, S. Tiburcius, S. M. Ruban, D. Shanbhag, C. I. Sathish, K. Ramadass, A. Vinu, *Emergent Mater.* **2019**, *2*, 337; d) J. Kossmann, D. Piankova, N. V. Tarakina, J. Heske, T. D. Kühne, J. Schmidt, M. Antonietti, N. López-Salas, *Carbon* **2021**, *172*, 497; e) W. Cai, J. Ding, Y. He, X. Chen, D. Yuan, C. Chen, L. Cheng, W. Du, H. Wan, G. Guan, *Energy Fuels* **2021**, *35*, 8857; f) P. Zhang, Y. Zhong, J. Ding, J. Wang, M. Xu, Q. Deng, Z. Zeng, S. Deng, *Chem. Eng. J.* **2019**, *355*, 963; g) A. Altwala, R. Mokaya, *Energy Adv.* **2022**, *1*, 216–224.

[18] a) C. Wang, L. Li, J. G. Bell, X. Lv, S. Tang, X. Zhao, K. M. Thomas, *Chem. Mater.* **2015**, *27*, 1502; b) B. Liu, S. Yao, X. Liu, X. Li, R. Krishna, G. Li, Q. Huo, Y. Liu, *ACS Appl. Mater. Interfaces* **2017**, *9*, 32820; c) L. Yang, X. Cui, Y. Zhang, Q. Wang, Z. Zhang, X. Suo, H. Xing, *ACS Sustainable Chem. Eng.* **2019**, *7*, 3138; d) L. Lei, Y. Cheng, C. Chen, M. Kosari, Z. Jiang, C. He, *J. Colloid Interface Sci.* **2022**, *612*, 132.

[19] R. Kodasma, J. Fermoso, A. Sanna, *Chem. Eng. J.* **2019**, *358*, 1351.

[20] a) S. K. Das, X. Wang, Z. Lai, *Microporous Mesoporous Mater.* **2018**, *255*, 76; b) S. K. Das, X. Wang, M. M. Ostwal, Y. Zhao, Y. Han, Z. Lai, *Chem. Eng. Sci.* **2016**, *145*, 21; c) H. Ma, H. Ren, X. Zou, S. Meng, F. Sun, G. Zhu, *Polym. Chem.* **2014**, *5*, 144.

[21] a) V. Presser, J. McDonough, S. H. Yeon, Y. Gogotsi, *Energy Environ. Sci.* **2011**, *4*, 3059; b) Z. Zhang, J. Zhou, W. Xing, Q. Xue, Z. Yan, S. Zhuo, S. Z. Qiao, *Phys. Chem. Chem. Phys.* **2013**, *15*, 2523.

[22] a) B. Liu, H. Li, X. Ma, R. Chen, S. Wang, L. Li, *RSC Adv.* **2018**, *8*, 38965; b) S. Khodabakhshi, M. Taddei, J. A. Rudd, M. J. McPherson, Y. Niu, R. E. Palmer, A. R. Barron, E. Andreoli, *Carbon* **2021**, *173*, 989.

[23] a) J. Li, L. Wang, Y. Zhao, S. Li, X. Fu, B. Wang, H. Peng, *Adv. Funct. Mater.* **2020**, *30*, 2001619; b) J. Li, K. Zhang, Y. Zhao, C. Wang, L. Wang, L. Wang, M. Liao, L. Ye, Y. Zhang, Y. Gao, B. Wang, H. Peng, *Angew. Chem. Int. Ed.* **2022**, *61*, e202114612.

[24] a) Y. Li, Y. Liang, H. Hu, H. Dong, M. Zheng, Y. Xiao, Y. Liu, *Carbon Carbon.* **2019**, *152*, 120; b) C. Long, J. Zhuang, Y. Xiao, M. Zheng, H. Hu, H. Dong, B. Lei, H. Zhang, Y. Liu, *J. Power Sources* **2016**, *310*, 145; c) J. Cheng, Q. Xu, X. Wang, Z. Li, F. Wu, J. Shao, H. Xie, *Sustainable Energy Fuels* **2019**, *3*, 1215; d) P. Lannelongue, R. Bouchal, E. Mourad, C. Bodin, M. Olarte, S. le Vot, F. Favier, O. Fontaine, *J. Electrochem. Soc.* **2018**, *165*, A657; e) J. Huang, Y. Liang, H. Hu, S. Liu, Y. Cai, H. Dong, M. Zheng, Y. Xiao, Y. Liu, *J. Mater. Chem. A* **2017**, *5*, 24775; f) H. Liang, T. Sun, L. Xu, C. Sun, D. Wang, *J. Mater. Sci. Mater. Electron.* **2019**, *30*, 13636; g) J. Yang, H. Wu, M. Zhu, W. Ren, Y. Lin, H. Chen, F. Pan, *Nano Energy* **2017**, *33*, 453.

Manuscript received: December 2, 2022
Accepted manuscript online: April 6, 2023
Version of record online: May 15, 2023